Physics Open 9 (2021) 100090

Contents lists available at ScienceDirect

Physics Open

journal homepage: www.elsevier.com/locate/physo

The effects of inhomogeneities on scroll-wave dynamics in an anatomically realistic mathematical model for canine ventricular tissue

K.V. Rajany [a,1], Rupamanjari Majumder [b], Alok Ranjan Nayak [c], Rahul Pandit [a,*,2]

[a] Centre for Condensed Matter Theory, Department of Physics, Indian Institute of Science, Bangalore 560012, India
[b] Department of Fluid Dynamics, Pattern Formation and Biocomplexity, Max Planck Institute for Dynamics and Self-Organization, Germany
[c] International Institute of Information Technology, Gothapatna, Po: Malipada, Bhubaneswar 751003, India

ARTICLE INFO

Keywords:
Cardiac arrhythmia
Scroll wave
Spiral wave dynamics
Ventricular fibrillation
Inhomogeneity

ABSTRACT

Ventricular tachycardia (VT) and ventricular fibrillation (VF) are lethal rhythm disorders, which are associated with the occurrence of abnormal electrical scroll waves in the heart. Given the technical limitations of imaging and probing, the *in situ* visualization of these waves inside cardiac tissue remains a challenge. Therefore, we must, perforce, rely on *in silico* simulations of scroll waves in mathematical models for cardiac tissue to develop an understanding of the dynamics of these waves in mammalian hearts. We use direct numerical simulations of the Hund–Rudy-Dynamic (HRD) model, for canine ventricular tissue, to examine the interplay between electrical scroll-waves and *conduction* and *ionic* inhomogeneities, in anatomically realistic canine ventricular geometries with muscle-fiber architecture. We find that millimeter-sized, distributed, conduction inhomogeneities cause a substantial decrease in the scroll wavelength, thereby increasing the probability for wave breaks; by contrast, single, localized, medium-sized ($\simeq$ cm) conduction inhomogeneities, exhibit the potential to suppress wave breaks or enable the self-organization of wave fragments into stable, intact scrolls. We show that ionic inhomogeneities, both distributed or localized, suppress scroll-wave break up. The dynamics of a stable rotating wave is not affected significantly by such inhomogeneities, except at high concentrations of distributed inhomogeneities, which can cause a partial break up of scroll waves. Our results indicate that inhomogeneities in the canine ventricular tissue are less arrhythmogenic than inhomogeneities in porcine ventricular tissue, for which an earlier *in silico* study (Majumder et al., 2016) has shown that the inhomogeneity-induced suppression of scroll waves is a rare occurrence.

1. Introduction

Life-threatening cardiac arrhythmias, such as ventricular tachycardia (VT) and ventricular fibrillation (VF), which are the leading cause of death in the industrialized world, are associated with unbroken (for VT) or broken (for VF) spiral or scroll waves of electrical activation in ventricular tissue [1–10]. The mechanisms leading to the formation of such scroll waves, their dynamics, and their interactions with other structural features in mammalian hearts continue to be an active area of research [9–18], for many different features can be arrhythmogenic. The heart has a complex, inhomogeneous structure and intricate geometry; it includes conducting tissue, with cardiac myocytes, non-conducting tissue, with fibroblasts, muscle fibers, a sheet structure, blood vessels, and scar tissues. The elucidation of the interactions of scroll waves of electrical activation with these multi-scale structures in cardiac tissue is required to develop (a) a detailed understanding of VT and VF and (b) possible defibrillation strategies, either pharmacological or electrical.

Experimental and numerical studies have shown that heterogeneities in cardiac tissue affect the dynamics of spiral or scroll waves and their break up (see, e.g., Refs. [9–14,17,18] and references therein), and thereby, both atrial and ventricular fibrillation. However, experiments on intact mammalian hearts are usually laborious, time-consuming, expensive, and still hampered by the considerable challenges in the visualization of electrical activity, below the tissue surface. [9–18]. Up until now, the experimental visualization of scroll filaments in the intact heart was only possible during fibrillation; a recent study [19] has used high-resolution, four-dimensional (4D), ultrasound-based imaging to map the occurrence of mechanical filamentous phase singularities that coexist with electrical phase singularities during cardiac fibrillation; 4D cardiac electromechanical

* Corresponding author.
E-mail addresses: rajanyk@iisc.ac.in (K.V. Rajany), rahul@iisc.ac.in (R. Pandit).
[1] Present address: S.A.R.B.T.M. Govt. College, Koyilandy, Calicut, India.
[2] Also at Jawaharlal Nehru Centre For Advanced Scientific Research, Jakkur, Bangalore, India.

https://doi.org/10.1016/j.physo.2021.100090
Received 4 November 2020; Received in revised form 15 January 2021; Accepted 25 August 2021
Available online 6 September 2021

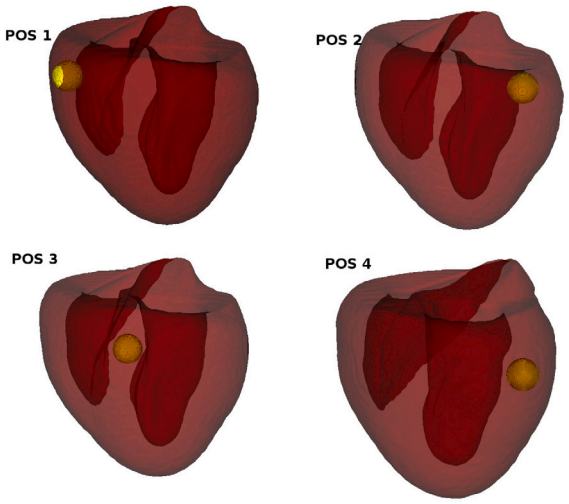

Fig. 1. The four illustrative positions of the localized, spherical inhomogeneities, inside the ventricular geometry, that we use for our simulations: One on the surface, partly inside and partly outside the tissue; one well inside the ventricular wall; one in the septum; we choose the last position, such that the scroll-wave filament comes close to the inhomogeneity during our numerical simulation.

activation imaging has also been used in Ref. [20]. Thus, numerical simulations or *in silico* studies, which use mathematical models for cardiac tissue, have become an increasingly promising alternative to *in vivo* and other experimental studies of scroll-wave dynamics in cardiac tissue.

In silico studies also give us great flexibility in changing individual parameter values (to explore, e.g., the effects of different medications on various ion-channel properties). However, such *in silico* studies are computationally challenging, especially if we use (a) physiologically realistic mathematical models, (b) anatomically realistic geometries, and (c) structural complexities like muscle-fiber orientation. It is not surprising, therefore, that many numerical studies use either simplified cardiac-tissue mathematical models or idealized geometries, e.g., a cubical domain or a wedge [7].

For reviews of the dynamics of scroll waves in the presence of structural and electrophysiological heterogeneities in cardiac tissue, we refer the reader to Refs. [2–5,8]. There have been studies of fiber-rotation-induced scroll-wave turbulence (see, e.g., Refs. [21–23] and references therein); in particular, they have investigated the effects of the anisotropy, because of fiber and sheet orientation, on such turbulence. Numerical studies, which use simplified models, have shown that an inhomogeneous excitable three-dimensional (3D) system, with a gradient of excitability, promotes twisting of the scroll waves, and can cause a simple scroll wave to change to a meandering scroll wave [24]. Thin, rod-like heterogeneities have been shown to suppress otherwise developing spatiotemporal chaos; furthermore, (a) they clear out already existing chaotic excitation patterns [25] and (b) spiral waves are either attracted towards or repelled from the centers of such inhomogeneities [26]. Computer-simulation studies have studied the effects of the structure of the heart on scroll waves in mathematical models [2–5]; for recent *in silico* studies of mathematical models for different mammalian hearts see, e.g., Refs. [27–29], for porcine- rabbit-, and human-ventricular models, respectively.

We investigate the interaction of scroll waves with two types of inhomogeneities in a realistic heart geometry for canine ventricles, conduction inhomogeneities and ionic inhomogeneities.

As a person ages, the concentration of nonconducting tissue increases because of fibrosis [30–34] and the formation of scars or dead tissue that act as conduction blocks [30–33]. These are the physiological equivalents of distributed conduction inhomogeneities and localized

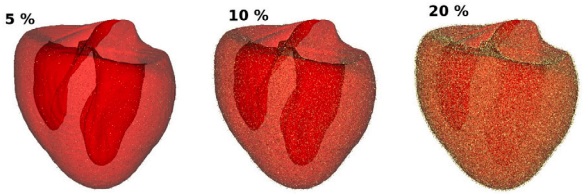

Fig. 2. The distribution of small-size inhomogeneities, inside the ventricular geometry that we use for our simulations The distribution of small-size inhomogeneities, inside the ventricular geometry that we use for our simulations: we employ three different concentrations (see text), namely, 5%, 10%, and 20%.

conduction inhomogeneities, respectively. Changes in different ionic conductivities do occur in mammalian hearts, in abnormal situations, or because of medicines or other external factors; these changes can be modeled as ionic inhomogeneities. Majumder, et al. have conducted a study of scroll-wave dynamics in a mathematical model for a pig heart with inhomogeneities [27]. In particular, they have studied the case in which the ventricle initially has a single rotating scroll wave; and they have then investigated how this single scroll evolves, as a result of the inhomogeneity that is introduced. We go beyond the study of Ref. [27] by including initial conditions that produce meandering as well as broken scroll waves, in the absence of inhomogeneities; we then let these waves evolve in the presence of inhomogeneities. Furthermore, we use a mathematical model for a dog heart instead of a pig heart. We compare the dynamics of scroll waves in these mathematical models for two different mammalian species, which have hearts of comparable sizes, but different electrophysiology. We find that inhomogeneities in the canine ventricular tissue are less arrhythmogenic than inhomogeneities in porcine ventricular tissue, for which an earlier *in silico* study [27] has shown that the inhomogeneity-induced suppression of scroll waves is a rare occurrence.

The remaining part of this paper is organized as follows. In Section 2 we present the model we use and the numerical methods we employ for our *in silico* study of this model. We discuss our results, for both conduction- and ionic-type inhomogeneities, in Section 3. We end with conclusions and a discussion of our results in Section 4.

2. Models and methods

For the canine-ventricular geometry that we use in our computations, we have downloaded diffusion-tensor magnetic-resonance-imaging (DTMRI) data from [35]; and we have then processed these data to produce our simulation geometry, with the locations of heart points and fiber directions.

We use the electrophysiologically detailed Hund–Rudy-Dynamic (HRD) model [36] for canine-ventricular myocytes to describe the dynamics at the cell level. The HRD model has 45 variables, including membrane and intercellular currents, gating variables, ionic concentrations, and the transmembrane potential V. We give a detailed description of this model in the Supplementary Material [37]. We use the monodomain approach for ventricular tissue; and the spatiotemporal evolution of the transmembrane potential V is given by the following partial-differential equation (PDE), which is of the reaction–diffusion type (all the other variables follow coupled ordinary differential equations (ODEs)):

$$\frac{\partial V}{\partial t} = \nabla . D \nabla V - \frac{I_{ion} + I_{applied}}{C_m}, \tag{1}$$

where I_{ion} contains all the ionic currents, $I_{applied}$ is the external current, C_m the capacitance density, and D the diffusion tensor that accounts for the conductivity of the tissue and propagation between cells; its elements are [38]:

$$D_{ij} = D_T * \delta_{ij} + (D_L - D_T)\alpha_i \alpha_j, \tag{2}$$

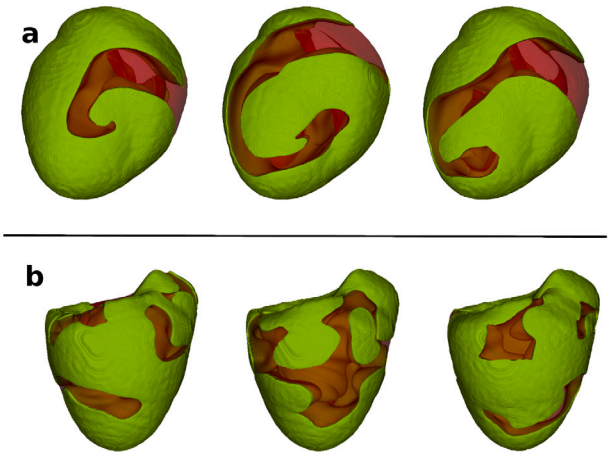

Fig. 3. Two-level isosurface plots of the transmembrane potential V illustrating the spatio-temporal evolution of scroll waves in the HRD model, in the anatomically realistic geometry for a canine ventricle (see text) and without any inhomogeneities. We use two different parameter sets: the first yields a rotating scroll wave (upper panel) and the second broken scroll waves interacting with each other (lower panel). For the full spatio-temporal evolution of V see the videos S41 (for the upper panel) and S42 (for the lower panel) in the Supplementary Material [41].

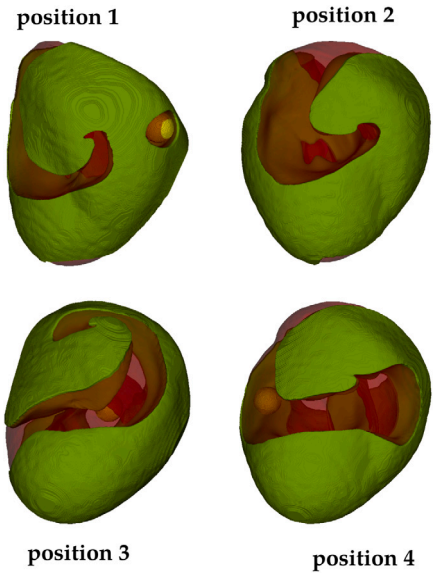

Fig. 4. Two-level isosurface plots of the transmembrane potential V illustrating scroll-wave dynamics, with a medium-sized spherical inhomogeneity of conduction type placed at position 1, 2, 3, and 4 in the domain (see Fig. 1). The initial configuration is obtained from the parameter set that produces a rotating scroll wave without the inhomogeneity; we depict the final configurations here. The rotating scroll is unaffected by the inhomogeneity. For the full spatio-temporal evolution of V see the videos S47 , S48 , S49 and S410 in the Supplementary Material [37].

where α is the vector describing the muscle-fiber direction, and D_L and D_T are the conductivities in the longitudinal and transverse fiber directions, respectively.

We impose Neumann boundary conditions by using the phase-field approach of Ref. [39] (see the Supplementary Material [37]). We solve the ODEs via the forward-Euler scheme and the PDEs by using a central-difference finite-difference method. We use a spatial resolution of 0.02 cm and a time step of 0.01 ms for our simulations. Such simulations are computationally challenging. To meet this challenge, we have developed an efficient CUDA code that we run on computer clusters that use graphics processing units (GPUs). This requires specialized programming [40]. We have checked our numerical results by comparing them with results for various ionic currents and the conduction velocity in the original HRD-model paper [36]. We have also carried out trial runs for a long time ($\simeq$ 10 s) to ensure the numerical stability of our results.

We consider the following two types of inhomogeneities in our HRD ventricular-tissue model: (a) conduction inhomogeneities because of a change in the diffusivity of the medium; we simulate these by setting the diffusion constant $D = 0$ at the locations of the inhomogeneities; (b) ionic inhomogeneities that arise from a change in any of the ionic properties across the cell membrane; in particular, we study ionic inhomogeneities by varying the L-type Calcium-ion-channel current I_{CaL} by reducing the value of the relevant parameter to $\gamma_{Cao} = 0.0314$. We have conducted extensive numerical studies with (a) medium-sized spherical inhomogeneities, located at four representative positions, as shown in Fig. 1, and (b) small-sized inhomogeneities, distributed throughout the simulation domain, with concentrations 5%, 10% and 20% of the whole volume of the tissue, as shown in Fig. 2.

With no inhomogeneity in our simulation domain, we have two types of scroll-wave dynamics: In the first case, there is a single, rotating, meandering scroll ($G_{Kr} = 5 \times 0.0138542$ and $\gamma_{Cao} = 3 \times 0.3410$); in the second, the scroll breaks up and its pieces interact with each other ($G_{Kr} = 3 \times 0.0138542$ and $\gamma_{Cao} = 1 \times 0.3410$) [42]. We illustrate these two types of scroll-wave dynamics, without any inhomogeneities, in Fig. 3. We now introduce inhomogeneities into our simulation domain to investigate how they affect the dynamics of these scroll waves. We study 28 cases in total. For each one of these cases we run our simulation for a time that is equivalent to 2.5 s in real time.

3. Results

In this Section, we present the results of our *in silico* studies. We first present the results of our simulations with conduction-type inhomogeneities, and then the results we have obtained with ionic-type inhomogeneities.

3.1. Conduction inhomogeneity: Effects on scroll-wave dynamics

Before we describe our results in detail, we refer the reader to Table 1, which summarizes our principal results for the effects of conduction-type inhomogeneities on scroll-wave dynamics.

Fig. 4 shows the final configuration of the evolution of scroll waves with a localized, spherical inhomogeneity (obstacle) of conduction type, for the four different, representative positions, on an initially rotating-scroll configuration. In this case we do not observe a qualitative change in the scroll-wave dynamics introduced by the inhomogeneity. The rotating scroll continues to rotate and is stable.

Fig. 5 shows the effects of a localized spherical inhomogeneity (obstacle) of conduction type on a broken-scroll configuration for four different positions of this obstacle. Panel a shows scroll-wave dynamics for position 1 of the inhomogeneity; we show isosurfaces of V at an early time as well as at the final stage: the broken scrolls slowly move away from the spherical inhomogeneity (depicted in yellow) and finally disappear from the medium. The panel-c shows the evolution of the scroll wave with the obstacle at position 2: We see that the broken scrolls have changed to a single rotating scroll; the scroll breaks up again because of the functional instabilities introduced by the parameter set we use; the broken scrolls again change to a rotating scroll; and the last snap-shot depicts another break up. Thus, in this case, the inhomogeneity prevents scroll break up; it changes broken scrolls into a single rotating scroll, which again breaks, and this keeps on repeating. The panel-b shows the spatio-temporal evolution of the scroll wave with the obstacle at position 3: here, the inhomogeneity cannot suppress the scroll breakup; in some regions it reduces the extent of break up, but it never completely changes the broken scrolls into a

Table 1
This table summarizes our results for the effects of conduction-type inhomogeneities on scroll-wave dynamics.

	Localized spherical inhomogeneity		Distributed small-scale inhomogeneities	
Broken scroll	Position1	Broken scrolls move away from the inhomogeneity and eventually move out of the domain.	**5%**	Rotating scroll with reduced wavelength.
	Position2	Breakup partially suppressed; broken scrolls change to a rotating scroll; it breaks again because of functional instability; and the cycle repeats.	**10%**	Wavelength reduces and break up occurs.
	Position3	Broken scrolls continue to break up and interact; scroll filament moves away from the inhomogeneity; breaking is not suppressed.	**20%**	Wavelength reduces significantly and break up is considerable.
	Position4	Breaking suppressed in the long run; and broken scrolls change to a rotating scroll.		
Rotating scroll	Position1	Continues rotating	**5%**	Wavelength reduces; and the scroll wave continues to rotate.
	Position2	Continues rotating	**10%**	Wavelength reduces and the scroll breaks up.
	Position3	Continues rotating	**20%**	Wavelength reduces by a large amount and there is considerable break up.
	Position4	Scroll continues rotating.		

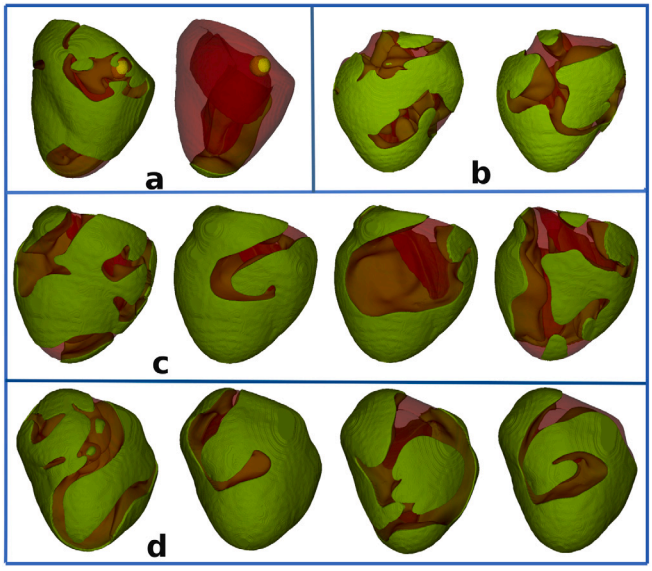

Fig. 5. Two-level isosurface plots of the transmembrane potential V illustrating the spatio-temporal evolution of scroll waves in the HRD model in the anatomically realistic canine ventricular geometry, when a medium-sized spherical inhomogeneity of conduction type is placed at the illustrative positions 1 (panel a), 3 (panel b), 2 (panel c), and 4 (panel d) shown in Fig. 1. The initial configuration is obtained from the parameter set that produces a broken scroll-wave state without the inhomogeneity; we depict the final configurations here. For the full spatio-temporal evolution of V see the videos S43 (for panel a), S44 (for panel b), S45 (for panel c) and S46 (for panel d) in the Supplementary Material [37].

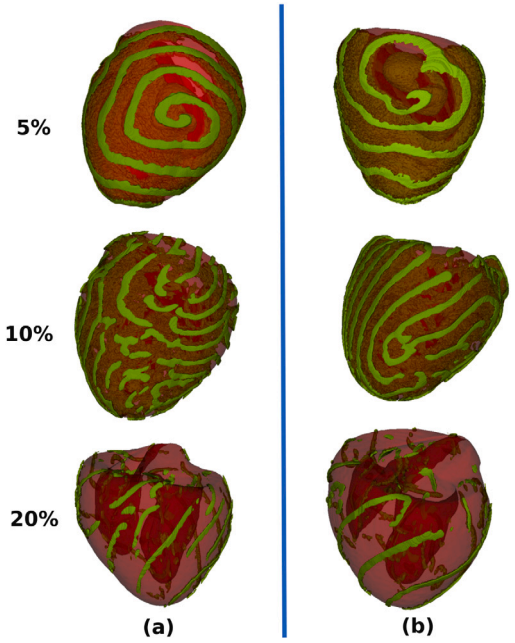

Fig. 6. Two-level isosurface plots of the transmembrane potential V illustrating the scroll-wave dynamics when small conduction inhomogeneities are distributed in the domain with concentration 5%, 10%, and 20% of the total number of sites. The initial configuration is obtained from the parameter set that produces a rotating-scroll state (left panel (a)) and a broken-scroll state (right panel (b)) a broken scroll-wave state, without the inhomogeneities; we depict the final configurations here. For the full spatio-temporal evolution of V see the videos S411, S412, S413 and S414, S415 and S416 in the Supplementary Material [37].

single scroll; the breakup of scrolls is considerable in this case. The lowest panel (d) shows the evolution of a scroll wave for position 4 of the inhomogeneity; in this case the broken scrolls are slowly changed to a single rotating scroll.

In summary, then, with the localized, medium sized conduction inhomogeneity, for initial conditions with a rotating scroll, the wave dynamics remains unchanged for all of the locations of the localized inhomogeneity. If the initial conditions produce broken scrolls, a localized inhomogeneity drives away the broken scrolls from the inhomogeneity; and the broken scrolls change into a rotating scroll, with its tip far away from the inhomogeneity for positions 1, 2, and 4. However, the presence of spherical inhomogeneity at position 3, i.e., at the septum, does not affect the broken scroll waves, which continue to break up. Thus, a medium-sized, spherical conduction inhomogeneity affects the scroll-wave dynamics slightly differently depending on its location: specifically, this dynamics depends on the relative distance between the phase-singularity line of the scroll wave and the position of the inhomogeneity. In general, such an inhomogeneity prevents scroll-wave break up, stabilizes broken scrolls into a single rotating scroll, and does not affect a single rotating scroll. If, however, the inhomogeneity is very far from the center of rotation, it cannot change the broken scrolls into a single rotating scroll.

We now present the results with small-sized, spherical inhomogeneities distributed throughout the simulation domain, with three different concentrations.

In Fig. 6 we show the spatiotemporal evolution of a scroll waves when we have distributed inhomogeneities, of the conduction type, for the following three different concentrations of inhomogeneities: 5%, 10%, and 20%.

In the left (panel (a)) we depict the spatio-temporal evolution of an initially rotating scroll wave. The wavelength of the scroll is reduced significantly. With a 5% concentration of the inhomogeneities,

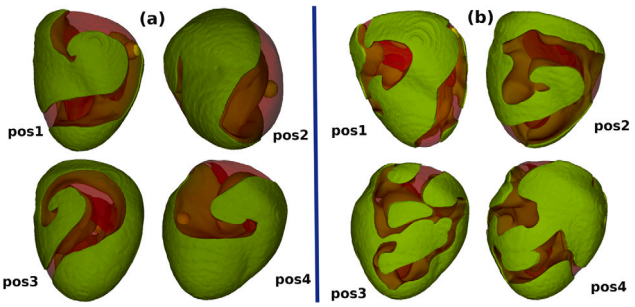

Fig. 7. Two-level isosurface plots of the transmembrane potential V illustrating the final state of the scroll-wave dynamics when a medium-sized spherical inhomogeneity, of ionic type, is placed at positions 1 (pos1), 2 (pos2), 3 (pos3), and 4 (pos4), as shown in Fig. 1. The initial configuration is the one that we obtain from the parameter set that yields a rotating scroll state for the left panel (a) and a broken-scroll-wave state for the right panel (b). For the full spatio-temporal evolution of V see the videos S417, S418, S419, and S420, S421 , S422, S423, and S424 in the Supplementary Material [37].

the wave does not break up; it continues rotating. For a 10% concentration of the inhomogeneities, the wave breaks up and forms a statistically steady broken-scroll state. With a 20% concentration of the inhomogeneities, the scroll breaks up to yield a statistically steady, broken-scroll state; the wavelength is reduced significantly.

With an initial parameter values which yield broken-scroll configuration, distributed conduction-type inhomogeneities have a marked effect on scroll-wave dynamics; in particular, the wavelength of the scroll is significantly reduced. With a 5% concentration of these inhomogeneities, the wave does not break up, but it rotates and curls up more than the initial configuration; in the last stages of this evolution, we see the two ends of the curled wave interacting with each other. With a 10% concentration of inhomogeneities, the wave breaks up immediately and we get a statistically steady broken-scroll state. When we have a 20% concentration of the inhomogeneities, the wave breaks up rapidly and it has a greatly reduced wavelength. As the percentage of inhomogeneities increases from 5% to 20% the drop in the wavelength and scroll-wave breakup is substantial.

3.2. Results for ionic inhomogeneity

Before we describe our results in detail, we refer the reader to Table 2, which summarizes our results for the effects of ionic-type inhomogeneities on scroll-wave dynamics. We have considered here all of the cases mentioned in the above section for conduction inhomogeneities.

In Fig. 7, panel (a) we show the effect of a localized, spherical inhomogeneity, of ionic type, on scroll-wave dynamics with an initial rotating-scroll configuration. For this initial condition, we find that the localized ionic inhomogeneities have no qualitative effect on the rotating scroll waves. The rotating scroll continues to rotate (Table 2). For position 3 we see the scroll center tends to move away from the inhomogeneity. We conclude, therefore, that scroll-wave dynamics is not affected substantially by the presence of localized ionic inhomogeneities when we use rotating-scroll initial conditions.

Fig. 7, panel (b) shows the effect of a localized, spherical inhomogeneity, of ionic type, on an initial configuration corresponding to broken-waves. If the ionic inhomogeneity is at positions 1 or 2, it partially prevents scroll breakup; and it stabilizes the dynamics to a single rotating scroll; but, for positions 3 and 4, the ionic inhomogeneity does not suppress the break up. Also, an ionic inhomogeneity does not completely remove the broken scrolls from the domain, as we have observed for position 1 for a conduction-type inhomogeneity.

We now examine the effects of distributed inhomogeneities, of ionic type, on two initial configurations in Fig. 8; for each case, we depict isosurfaces of V from the last stage of our simulation. For small-sized,

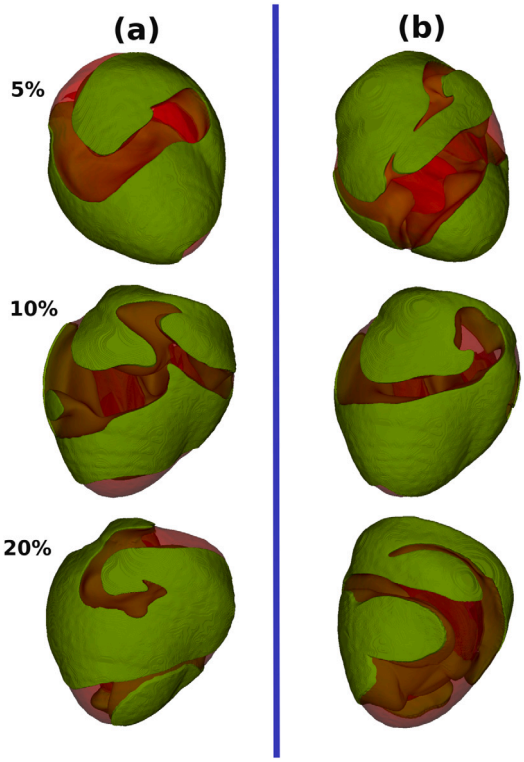

Fig. 8. Two-level isosurface plots of the transmembrane potential V illustrating scroll-wave dynamics, when small ionic inhomogeneities are distributed in the domain with a concentration 5%, 10% and 20% of the total number of sites. The initial configuration corresponds to the parameter set that yields, in the absence of inhomogeneities, a rotating scroll wave [panel (a)], and scroll wave break-up [panel (b)]. For the full spatio-temporal evolution of V see the videos S425, S426, S427, S428, S429, and S430 in the Supplementary Material [37].

distributed inhomogeneities, with a rotating-scroll initial configuration, we see that (as in the case of conduction inhomogeneities), for small concentrations of inhomogeneities (5%), the rotating scroll wave is unaffected by them; but, as this concentration increases, the inhomogeneities cause the rotating scroll to break up. The break up is not as fast, intense, or statistically steady, as in the case of conduction inhomogeneities. Furthermore, here the wavelength of the scrolls does not change (as it does for conduction inhomogeneities). We observe that the extent of such break up is more for 10% inhomogeneities than for 20%.

Fig. 8, panel (b), shows the effects on scroll-wave dynamics, of distributed inhomogeneities of ionic type, for an initial broken-scroll configuration. We observe that, for 10% distributed inhomogeneities, the scroll break up is partially suppressed. In other cases the such break up is not suppressed.

We conclude that the effect of ionic-type inhomogeneities on scroll-wave dynamics of broken scrolls are different, in detail, from those of conduction-type of inhomogeneities. For distributed, small-sized inhomogeneities, conduction inhomogeneities break up the scrolls significantly; ionic inhomogeneities prevent scroll-wave break up for moderate(10%) concentration of inhomogeneities. Localized inhomogeneities have almost the same effect on scroll-wave dynamics as conduction-type obstacles. At two positions (1 and 2), they prevent the breaking up of scrolls by partially changing broken waves to rotating scrolls. For ionic inhomogeneities at positions 3 and 4, we do not see this behavior. Thus, scroll-wave dynamics also depends on the position of the inhomogeneity. Finally, we note that a localized ionic inhomogeneity does not have a significant effect on an initially rotating scroll wave as in the case of localized conduction inhomogeneity.

Table 2
This table summarizes our results on the effects of ionic-type inhomogeneities on scroll-wave dynamics.

	Localized spherical inhomogeneity		Distributed small-scale inhomogeneities	
Broken scroll	Position 1	Broken scroll filaments tend to move away from the inhomogeneity; partially; suppresses scrolls break-up.	**5%**	Does not suppress scroll-wave break up.
	Position 2	Same dynamics as for position 1.	**10%**	Reduces scroll-wave break-up, but does not suppress it completely.
	Position 3	Does not suppress break up; broken scrolls continues to break up.	**20%**	Does not suppress scroll wave break-up.
	Position 4	Same dynamics as for position 3.		
Rotating scroll	Position 1	Continues rotating.	**5%**	Continues rotating; meandering is increased.
	Position 2	Continues rotating.	**10%**	Scroll wave breaks-up occurs.
	Position 3	Continues rotating; the scroll tends to move away from the inhomogeneity.	**20%**	Scroll rotates for a long time without breaking, finally break-up occurs.
	Position 4	Continues rotating.		

4. Conclusions

We have carried out a detailed *in silico* study to examine the effects of different types of inhomogeneities on scroll-wave dynamics in dog ventricles. Our work goes well beyond earlier studies because we have used an anatomically realistic model for canine ventricles, namely, the HRD model; and we have also included muscle-fiber orientation. Our study has elucidated the effects of *conduction* and *ionic* inhomogeneities on scroll waves in this model. The mathematical model that we use is realistic insofar as we account for detailed ion-channel dynamics and tissue anisotropy, with standard values for conductivities in parallel and perpendicular directions. We give details in the Supplementary Material (e.g., D_L in Eq. (2) is 2 cm^2/s for the HRD model and the ratio $D_L : D_T = 4 : 1$, which is comparable to the experimentally recorded ratios). In particular, we have found that small-scale, distributed, conduction inhomogeneities have the most marked effect on scroll-wave dynamics: these inhomogeneities reduce the wavelength significantly at all concentrations. Low concentration of the inhomogeneities ($\simeq$ 5%) do not break up the scroll wave; but higher concentrations (10% and above) do break up the rotating scroll and, indeed, break up the broken scrolls too. A localized, large-scale conduction inhomogeneity, partially suppresses wave break ups and stabilizes broken waves to form a rotating wave (for most positions of the inhomogeneity); and it does not affect the break up of scrolls in one position (in the septum). However, if the medium already has a stable rotating wave, the presence of such inhomogeneities does not affect the wave dynamics.

We find, for the ionic inhomogeneities that we have studied, at medium (10%) concentrations of distributed, small-scale inhomogeneities partially suppress scroll-wave break up; at other concentrations, the such inhomogeneities do not affect the broken waves. Higher (10% and above) concentrations of distributed inhomogeneities, can cause the partial break up of initially rotating scroll waves; and low concentrations do not affect the scroll-wave dynamics. A localized, large-scale, ionic-type inhomogeneity stabilizes the broken-wave dynamics at two positions; and it does not affect the dynamics when it is at the other positions (see above). The dynamics of a stable rotating wave is not affected significantly by localized ionic inhomogeneities. The scrolls tend to move away from local inhomogeneities of both conduction and ionic types. When the position of the inhomogeneity is away from the region of the phase singularity of the scrolls, it does not suppress the break up significantly.

In summary, our study shows that localized conduction inhomogeneities can suppress scroll-wave break up and chaos, to some extent; and distributed, conduction inhomogeneities can lead to a statistically steady broken-wave state with spatiotemporal chaos. Stable rotating scrolls in the medium are not affected by localized inhomogeneities, but are broken by distributed inhomogeneities at high concentrations, for both conduction and ionic types of inhomogeneities. Ionic type inhomogeneities can suppress scroll-wave break up.

Our results can be compared fruitfully with a similar *in silico* study [27] of scroll-wave dynamics in a mathematical model for a pig heart. This study also finds that small-scale, distributed, conduction inhomogeneities have the most marked effect on scroll-wave dynamics, as we have found for the HRD canine-ventricular model. The main findings of the above study are conduction-type inhomogeneities become increasingly important, in the case of multiple, randomly distributed, obstacles at the cellular scale (0.2 mm $-$0.4 mm). Such configurations can lead to scroll-wave break up; and ionic inhomogeneities affect scroll-wave dynamics significantly at large length scales, when these inhomogeneities are localized in space at the tissue level (5 mm $-$10 mm). In such configurations, these inhomogeneities can (a) attract scroll waves, by pinning them to the heterogeneity, or (b) lead to scroll-wave breakup. The authors of Ref. [27] used an initial configuration with a stable rotating spiral. They found no qualitative change in the dynamics of such a wave when small-scale ionic distributed inhomogeneities were introduced and also when large, localized conduction inhomogeneities were included.

We also find that large, localized, conduction inhomogeneities do not affect a stable rotating wave. Thus, for such inhomogeneities, our results match with those for this pig-heart study [27], with the same initial conditions. We study broken-wave initial conditions too. For ionic inhomogeneities, our HRD-model studies show that the stable rotating wave finally breaks up for large concentration of distributed inhomogeneities; this is in contrast to pig-heart study of Ref. [27], in which such a wave is not significantly affected by these inhomogeneities. Conduction inhomogeneities affect the diffusion part of the governing equations; this is the same for all models, so the results also turn out to be the same for canine- and porcine-ventricular models. The reaction part of the equations is model specific; and the ionic inhomogeneities that are used in these two studies also have different conductances; thus, the results, with such inhomogeneities, are model specific. In the porcine-model study [27] of Majumder, et al. we did see some cases with scroll waves pinned to the inhomogeneity. However, in our canine-heart simulations we do not see such scroll-wave pinning at the inhomogeneity.

With the types of localized inhomogeneities we have investigated, canine ventricles have a lower tendency to be in the arrythmogenic region, with broken scroll waves, compared to porcine ventricles (as illustrated in the study [27] by Majumder, et al.). The principal reason for this is the following major difference between canine and porcine cardiac myocytes: the APD restitution curve, for a porcine-model myocyte, is sharp with slope greater than one in the scroll-break-up region; by contrast, for the canine-model myocyte, the APD restitution curve has a much smaller slope less than one. We demonstrate this in the Supplementary Material. This sharp restitution curve makes porcine ventricles more prone to scroll break up than the canine myocytes in the HRD model, where the maximal slope of the APD restitution curve is $\simeq$ 0.15.

We mention some limitations of our study. We have not included Purkinje fibers, the His bundle, and mechanical deformation of the ventricles in our study. Their presence is important (see, e.g., Refs. [43,44] for Purkinje Fibers and Refs. [45–49] for mechanical deformation), but a detailed study of their effects lies beyond the scope of the present study, which focuses on the effects of localized inhomogeneities on

scroll-wave dynamics in the HRD model. We have used a monodomain model for the cardiac-tissue equations in our study; bidomain models are more realistic than monodomain ones; however, a recent study [50] has shown that the latter are adequate when currents are low, as in our study. To impose boundary conditions we have used a phase-field approach; this can also be done with a finite-element model, which we leave for future work. The inhomogeneities could be handled in a more realistic way than in our study in terms of shape, composition, etc.

We hope our work will lead to other detailed studies of scroll-wave dynamics in realistic models for mammalian hearts. Only by contrasting the results of such studies can we develop a detailed understanding of VT and VF, which is a prerequisite for the efficient elimination (i.e., defibrillation) of such life-threatening cardiac arrhythmias.

CRediT authorship contribution statement

K.V. Rajany: Software, Formal analysis, Visualization, Writing - original draft. **Rupamanjari Majumder:** Conceptualization, Methodology, Data curation. **Alok Ranjan Nayak:** Investigation, Validation. **Rahul Pandit:** Resources, Supervision, Validation, Writing - review and editing, Funding acquisition.

Declaration of competing interest

The authors declare that they have no known competing financial interests or personal relationships that could have appeared to influence the work reported in this paper.

Acknowledgments

We thank Council of Scientific and Industrial Research, India, University Grants Commission and Department of Science and Technology for support, and Supercomputing Education and Research Centre (IISc) for computational resources, India.

Appendix A. Supplementary data

Supplementary material related to this article can be found online at https://doi.org/10.1016/j.physo.2021.100090.

References

[1] J.M. Davidenko, J. Cardiovascul. Electrophysiol. 4 (1993) 730–746, 6.
[2] R. Clayton, A. Panfilov, Prog. Biophys. Mol. Biol. 96 (2008) 19–43.
[3] R.H. Clayton, O. Bernus, E.M. Cherry, H. Dierckx, F.H. Fenton, L. Mirabella, A.V. Panfilov, F.B. Sachse, G. Seemann, H. Zhang, Prog. Biophys. Mol. Biol. 104 (2011) 22–48.
[4] N.A. Trayanova, Circ. Res. 108 (2011) 113–128.
[5] E.M. Cherry, F.H. Fenton, New J. Phys. 10 (2008).
[6] J. Keener, J. Sneyd, Mathematical Physiology, Springer, New York, 1998.
[7] A. Pertsov, M. Vinson, Phil. Trans.: Phys. Sci. Eng. 347 (1994) 687–701, 1685.
[8] J.N. Weiss, A. Garfinkel, et al., J. Mol. Cell. Cardiol. 82 (2015).
[9] R. Majumder, A.R. Nayak, R. Pandit, Heart Rate and Rhythm, Springer, 2011, pp. 269–282.
[10] T.K. Shajahan, S. Sinha, R. Pandit, in: S.K. Dana, P.K. Roy, J. Kurths (Eds.), Complex Dynamics in Physiological Systems: from Heart to Brain, in: Understanding Complex Systems, Springer, Dordrecht, 2009, pp. 51–67.
[11] R. Majumder, A.R. Nayak, R. Pandit, PLoS One 7 (2012) e45040.
[12] R. Majumder, A.R. Nayak, R. Pandit, PLoS One 6 (2011) e18052, 4.
[13] A.R. Nayak, R. Pandit, Front. Physiol. 5 (2014) 207.
[14] A.R. Nayak, T.K. Shajahan, A.V. Panfilov, R. Pandit, PLoS One 8 (2013) e72950, 9.
[15] T. Ikeda, M. Yashima, T. Uchida, D. Hough, M.C. Fishbein, et al., Circ. Res. 81 (1997) 753.
[16] Z.Y. Lim, B. Maskara, F. Aguel, R. Emokpae Jr., L. Tung, Circulation 114 (2006) 2113–2121.
[17] T.K. Shajahan, S. Sinha, R. Pandit, Phys. Rev. E 75 (2007) 011929-1–011929-8.
[18] T.K. Shajahan, A.R. Nayak, R. Pandit, PLoS One 4 (2009) e4738, 3.
[19] J. Christopher, M. Chebbok, C. Richter, et al., Nature 555 (2018) 667–672.
[20] J. Grondin, D. Wang, C.S. Grubb, N. Trayanova, E.E. Konofagoua, Comput. Biol. Med. 113 (2019) 103382.
[21] F. Fenton, A. Karma, Phys. Rev. Lett. 81 (1998) 481–484.
[22] F. Fenton, A. Karma, Chaos 8 (1998) 20–47.
[23] R. Majumder, A.R. Nayak, R. Pandit, PLoS One 6 (2011) e18052, 4.
[24] Z. Yang, S. Gao, Q. Ouyang, H. Wang, Phys. Rev. E 86 (2012) 056209.
[25] F. Spreckelsen, D. Hornung, O. Steinbock, U. Parlitz, S. Luther, Phys. Rev. E 92 (2015) 042920, 4.
[26] P. Kuklik, P. Sanders, L. Szumowski, J.J. Zebrowski, J. Biol. Phys. 39 (2013).
[27] R. Majumder, R. Pandit, A.V. Panfilov, JETP Lett. 104 (2016) 796–799, 11.
[28] S.K. Galappaththige, P. Pathmanathan, M.J. Bishop, R.A. Gray, Front. Physiol. 10 (2019) 564.
[29] S. Zimik, R. Pandit, R. Majumder, PLoS One 15 (2020) e0230214, 3.
[30] Anna Biernacka, N.G. Frangogiannis, Aging Dis. 158 (2011).
[31] Augusto Orlandi, et al., Cardiovasc. Res. 64 (3) (2004) 544–552.
[32] Lu Lu, et al., Clin. Exp. Pharmacol. Physiol. 44 (2017) 55–63.
[33] Sanne De Jong, et al., J. Cardiovascul. Pharmacol. i57 (6) (2011) 63–638.
[34] Ten Tusscher, H.W.J. Kirsten, A.V. Panfilov, Europace 9 (2007) vi38–vi45.
[35] http://cmiss.bioeng.auckland.ac.nz.
[36] T. Hund, Y. Rudy, Circulation 110 (2004) 20.
[37] K.V. Rajany, Supplementary Material, IISc, Bangalore.
[38] K.H.W.J ten Tusscher, O. Bernus, R. Hren, A.V. Panfilov, Prog. Biophys. Mol. Biol. 90 (2006) 326–345.
[39] F.H. Fenton, E.M. Cherry, A. Karma, W.J. Rappel, Chaos 15 (2005) 013502.
[40] K.V. Rajany, Numerical studies of spiral- and scroll-wave dynamics in cardiac tissue (Doctoral thesis), Indian Institute of Science, Bangalore, India, 2020, unpublished.
[41] K.V. Rajany, Movies showing the spatiotemporal evolution of the various systems in this study, see section 2 of the Supplementary Material, IISc. Bangalore.
[42] K.V. Rajany, A.R. Nayak, R. Majumder, R. Pandit, Rapid-rectifier-potassium and L-type-calcium currents play a crucial role in spiral- and scroll-wave dynamics in mathematical models for canine and human ventricular tissue (unpublished); see Chapter 3 of Ref. [40].
[43] A.R. Nayak, A.V. Panfilov, R. Pandit, Phys. Rev. E 95 (2017) 022405.
[44] M.E. Mangoni, J. Nargeot, Physiol. Rev. 88 (2008) 919.
[45] A.R. Nayak, R. Pandit, Front. Physiol. 5 (2014) 207.
[46] H. Zhang, B. Li, Z. Sheng, Z. Cao, G. Hu, Europhys. Lett. 76 (2006).
[47] H. Zhang, X. Ruan, B. Hu, Q. Ouyang, Phys. Rev. E 70 (2004).
[48] L.D. Weise, M.P. Nash, A.V. Panfilov, PLoS One 6 (2011).
[49] J. Chen, J. Xu, X. Yuan, H. Ying, J. Phys. Chem. B 113 (2008) 849–853.
[50] M. Potse, B. Dube, J. Richer, A. Vinet, R.M. Gulrajanii, IEEE Trans. Biomed. Eng. 53 (2006) 12.